CrossMark

Influence of $La_2Zr_2O_7$ Additive on Densification and Li^+ Conductivity for Ta-Doped $Li_7La_3Zr_2O_{12}$ Garnet

XIAO HUANG,[1] CHEN SHEN,[1] KUN RUI,[1] JUN JIN,[1] MEIFEN WU,[1] XIANGWEI WU,[1] and ZHAOYIN WEN[1,2]

1.—CAS Key Laboratory of Materials for Energy Conversion, Shanghai Institute of Ceramics, Chinese Academy of Science, 1295 DingXi Road, Shanghai 200050, People's Republic of China. 2.—e-mail: zywen@mail.sic.ac.cn

A high-conductivity solid electrolyte, $La_2Zr_2O_7$ (LZO) added to $Li_{6.4}La_3Zr_{1.4}Ta_{0.6}O_{12}$ (LLZTO), was prepared via conventional solid-state reactions and sintered at 1100°C for 10 h, which is tens of Celsius degrees lower than the typical sintering temperature for LLZTO. The addition of LZO did not bring in any impurities. LZO acted as a sintering aid to densify the LLZTO from a relative density of 77% up to 90%, which was comparable to that of pure LLZTO sintered at 1200°C. The 6 wt.% LZO–LLZTO samples sintered at 1100°C and 1200°C exhibited a room-temperature conductivity of 1.92×10^{-4} S/cm and 5.84×10^{-4} S/cm, respectively, which were higher than that of pure LLZTO samples. Glass-like phases observed at grain boundaries in LZO–LLZTO ceramics indicated that LZO promoted the formation of the glass-like phases binding together LLZTO grains and thus leading to enhanced density and conductivity of LLZTO.

INTRODUCTION

High-energy and long-life Li-ion batteries (LIBs) have been in great demand for portable electronic devices and electric vehicles.[1] Solid-state Li-ion, Li–S and Li-air batteries containing solid-state electrolytes have attracted great attention, due to their high energy density and safety compared with lithium batteries using liquid organic electrolytes.[2-6] Different types of solid electrolytes, including NASICON-type phosphates,[7,8] LISICON-type sulfides[9,10] and their glass–ceramic analogs,[11,12] perovskite-type titanates,[13] Li_3N, LiPON and the new but promising $Li_7La_3Zr_2O_{12}$(LLZO) garnets[14] have been reported. Among them, cubic garnet phase LLZO is chemically and electrochemically stable against Li metal electrodes, showing a total ionic conductivity above 10^{-4} S/cm at room temperature and a wide electrochemical potential window of 6 V,[15] which makes it a promising electrolyte candidate for solid-state LIBs. Elements like Al, Ga, Y, Si, Ge, Nb, Ta and Te have been doped in order to stabilize the cubic phase and improve ionic conductivity of LLZO. Among them, Ta-doped LLZO shows a lithium ionic conductivity of 1×10^{-3} S/cm, which is much higher than that of undoped LLZO.[16]

For the successful application of LLZTO as solid electrolyte membrane in solid-state batteries, a dense microstructure related to grains and grain boundaries is a critical issue. An increase in Li^+ conductivity (bulk + grain boundary) is expected for LLZTO with a denser microstructure due to the reduction in the grain boundary resistance. In addition, formation of lithium dendrites during cycling of solid-state batteries can be completely inhibited by dense ceramic electrolytes. A high reaction temperature and long sintering time are required for the preparation of highly conductive and dense LLZTO via conventional solid-state methods.[16] To overcome these difficulties, wet chemical techniques have been employed for relatively lower reaction and sintering temperatures, as well as shorter sintering times.[17] The hot-pressing technique has also been adopted to obtain dense LLZTO electrolytes at a lower sintering temperature.[18] However, these methods are always expensive and less productive. Therefore, incorporation with sintering aids is an effective strategy to lower the sintering temperature for garnets, such as the composite with an Al-contaminant from Al_2O_3 crucibles[19] and those with the additives Li_3BO_3, Li_3PO_4 and Li_4SiO_4.[20] Rao et al.[21] revealed that mixed

Li_2CO_3, La_2O_3 and ZrO_2 would first react with each other to form $La_2Zr_2O_7$ (LZO) phase at 800°C during the solid-state reaction process. Then, LZO would be lithiated to LLZO at higher temperatures and pure LLZO phase formed at 980°C. LZO was the reaction precursor for cubic LLZO during the solid-state reaction process. LZO would react with excess Li_2O from LLZTO green pellets and external bed powder, which was always employed to compensate Li loss during high-temperature sintering[15] and form highly active glass-like phases which could act as sintering aids to densify LLZTO ceramics.

In this work, systematic investigations have been carried out on the preparation of high Li^+ conductive LLZTO in cubic phase by cheap and productive solid-state reaction methods. LLZTO pellets incorporated with different amounts of LZO were obtained by sintering them under various conditions. The phase, relative density and electrochemical performance of sintered LLZTO–LZO pellets were carefully studied and the influence of LZO addition on the relative density and Li^+ conductivity are discussed in detail. We also observed the microstructure of the cross-section of these samples and conducted $LiOH\cdot H_2O$-LZO solid-state reaction experiments to reveal the reaction of LZO inside the pellets during sintering process. A possible mechanism has been proposed for the effect of LZO on promoting densification of LLZTO ceramics.

EXPERIMENTAL

Synthesis

Sub-micron $La_2Zr_2O_7$ (LZO), bed powder $Li_{6.75}La_3Zr_{1.75}Nb_{0.25}O_{12}$ (LLZNO) and $Li_{6.4}La_3Zr_{1.4}Ta_{0.6}O_{12}$ (LLZTO) were prepared by conventional solid-state reactions and details can be found in the online supporting materials.

An amount of 0–10 wt.% sub-micron LZO was added to the as-prepared LLZTO powder and then ground at 250 rpm for 6 h to a size of several micrometers, which was much larger than the size obtained by the wet chemical process or the high speed attrition milling method. The slurry was dried at 70°C overnight and the obtained powder was marked as LLZTO–xLZO (x = 0–10 wt.%) for different weight ratios of added LZO. These powders were dry-pressed into Φ14 mm × 2 mm green pellets and then isostatically pressed under 200 MPa. Green pellets with different weight ratios of LZO were sintered at 1050°C × 20 h, 1100°C × 10 h, 1150°C × 5 h, 1200°C × 2.5 h with excess $Li_{6.75}La_3Zr_{1.75}Nb_{0.25}O_{12}$ as the bed powder to provide a Li_2O atmosphere during the high-temperature process.

In order to understand the reaction mechanism of LZO with Li_2O, raw materials with the weight ratios of 1:1 and 1:2 for $LiOH\cdot H_2O$ to LZO were mixed at 250 rpm for 16 h and dried overnight. After sieving over 200-mesh screen, the powders were pressed into Φ18 mm × 2 mm pellets and sintered at 1150°C × 5 h under the same conditions as the LLZTO–LZO green pellets.

Characterization

The granularity distribution of attrition-milled LZO particles and ball-milled LLZTO particles were analyzed by a laser particle size analyzer (Mastersizer 2000; Malvern). Powder x-ray diffraction (Ultima IV, nickel-filtered Cu-Kα radiation, λ = 0.1542 nm; Rigaku) was employed to determine the phase component of the samples at room temperature in the 2θ range of 10°–70° with the step of 0.1°/s. Scanning electron microscopy (SEM; HITACHI S-3400 N) was used to examine the morphology of the cross-section of the as-prepared LLZTO–xLZO (x = 0–10%) samples. The densities of the sintered pellets were measured at room temperature (22.4°C) with the Archimedes method using alcohol as the immersion medium with Mettler–Toledo density measurement attachments. The theoretical density was calculated from the X-Ray Diffraction (XRD) results. The ionic conductivity was measured at 25°C by AC impedance analysis (Model PGSTAT302 N; Autolab). The potentiostatic impedance of the frequency resistance analysis was selected as the test model, while the frequency ranged within 1 MHz–10 Hz and the electrical perturbation was set to 20 mV. Before the tests, both parallel surfaces were sputtered with gold as the lithium ion blocking electrode.

RESULTS AND DISCUSSION

Powder Analysis

The particle size distribution for attrition-milled LZO powder is shown in Fig. 1a. The D(50) and D(90) of attrition-milled LZO particles were 0.198 μm and 0.308 μm, respectively, which were confirmed by the SEM image (Fig. 1b). The particle size distribution was bimodal. The main peak at ~0.2 μm corresponded to the primary particles and the minor smaller peak at ~0.65 μm corresponded to the agglomerated particles, which were observed in the SEM image. The XRD patterns are shown in Fig. 1c. The diffraction peaks of as-synthesized powder corresponded to the standard pyrochlore LZO phase (PDF#50-0837). However, when well-crystallined coarse powder was ground to fine sub-micron particles, the diffraction intensity was lower because of the weaker surface crystallinity of the milled particles. The width of the peak was also broader. The lower diffraction intensity and broader diffraction peaks of attrition-milled LZO were in good agreement with the granularity analysis and SEM image.

The particle size distribution for ball-milled LLZTO powder as shown in Fig. 2a. The D(50) and D(90) of ball-milled LLZTO–LZO particles were 3.362 μm and 8.241 μm, respectively, which were

Influence of La$_2$Zr$_2$O$_7$ Additive on Densification and Li$^+$ Conductivity for Ta-Doped Li$_7$La$_3$Zr$_2$O$_{12}$ Garnet

2595
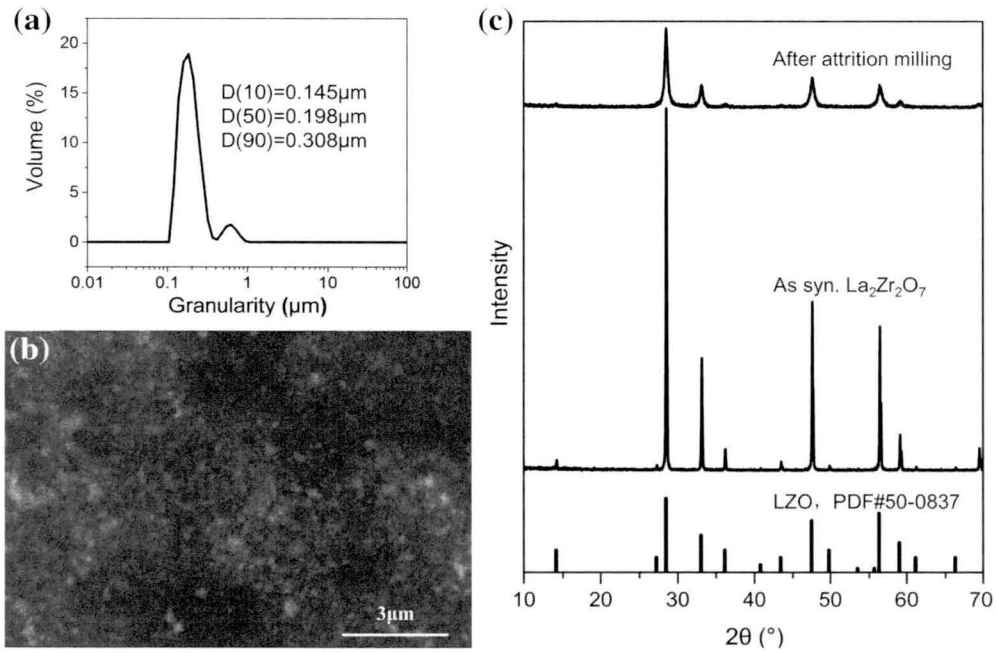
Fig. 1. The particle size distribution (a) and SEM image (b) of attrition-milled LZO powder. (c) XRD patterns of as-synthesized LZO and powder after attrition milling.
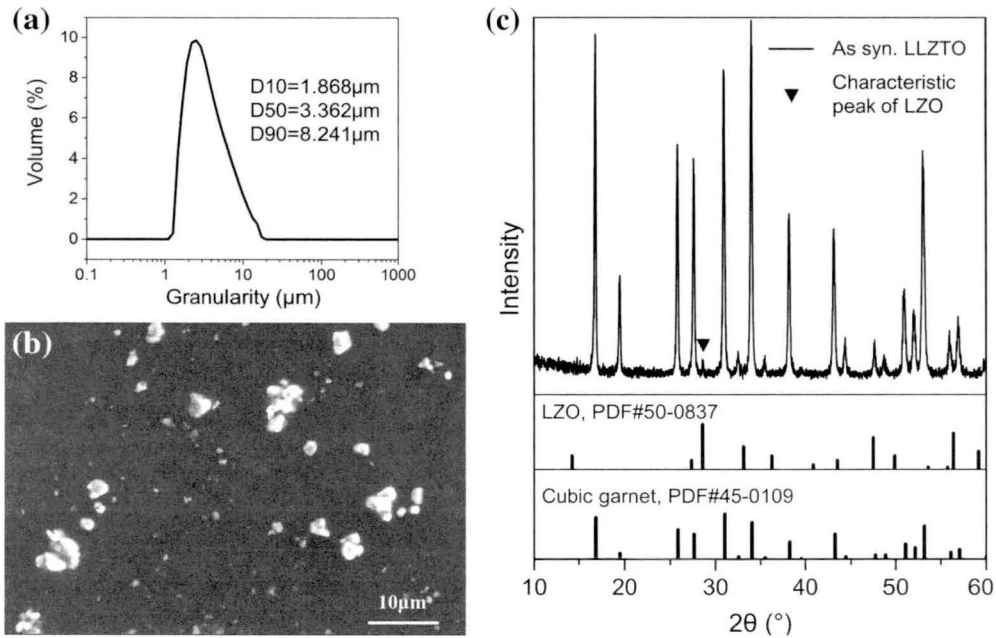
Fig. 2. The particle size distribution (a) and SEM image (b) of ball-milled LLZTO powder. (c) XRD pattern of as-synthesized LLZTO.

also confirmed by SEM image (Fig. 2b). The particle size distribution was unimodal. The XRD pattern is shown in Fig. 2c. The main diffraction peaks of the as-synthesized LLZTO powder coincided with the cubic garnet phase. The triangle-marked peak corresponds to LZO. The weak intensity of the LZO impurity indicated a very small amount of LZO in LLZTO powder, which was negligible compared with that in the added attrition-milled LZO. The combination of coarse LLZTO particles with low activity and fine sub-micron LZO particles with high activity would straightforwardly show the effect of LZO on promoting densification of LLZTO ceramics.

(a)

(b)

(c)

(d)
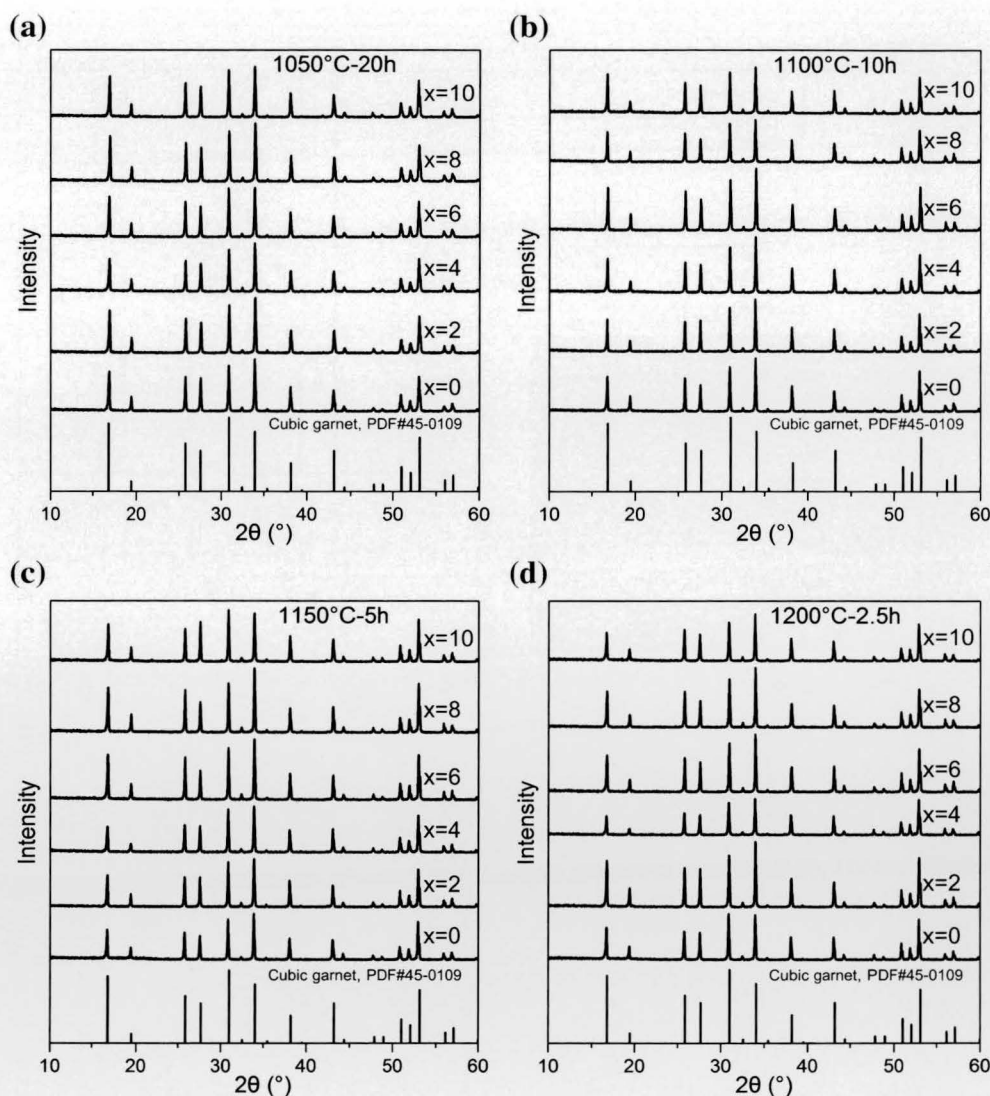
Fig. 3. XRD patterns of LLZTO–xLZO (x = 0–10 wt.%) pellets sintered under different conditions: (a) 1050°C × 20 h; (b) 1100°C × 10 h; (c) 1150°C × 5 h; (d) 1200°C × 2.5 h.

Analysis of Sintered Ceramics

All sintered pellets were pure cubic garnet phase as shown in Fig. 3, even for the samples with a LZO ratio of 10 wt.% sintered at 1050°C (Fig. 3a). No peaks related to LZO were observed for any of the samples, indicating that there was no LZO left or that the remaining amount of LZO was too small to be detected by XRD. This phenomenon pointed out that the LZO reacted with some other materials during the high-temperature sintering process.

The theoretical density of LLZTO–LZO pellets was calculated to be ~5.5 g/cm^3 based on XRD data. The relative density was determined by the ratio of measured density to theoretical density. Relative density was plotted versus the weight ratio of the LZO additive and shown in Fig. 4. At a low sintering temperature of 1050°C, no samples were sintered and the relative density was much lower than 70%. However, the LLZTO–4LZO samples showed ~13%
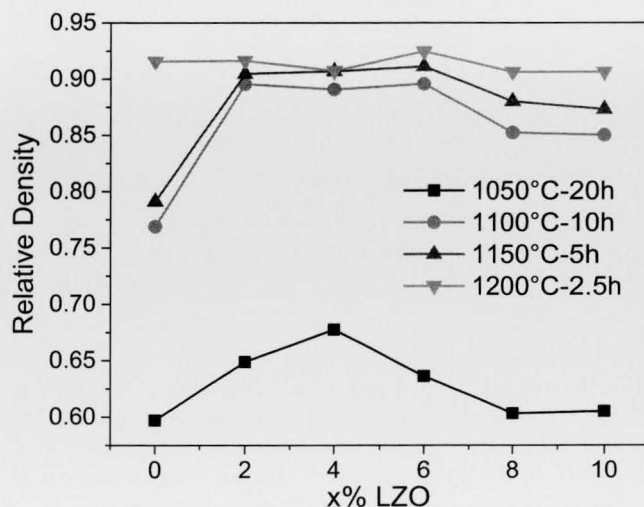
Fig. 4. Relative density of LLZTO–xLZO (x = 0–10 wt.%) pellets sintered under different conditions.

Influence of La$_2$Zr$_2$O$_7$ Additive on Densification and Li$^+$ Conductivity for Ta-Doped Li$_7$La$_3$Zr$_2$O$_{12}$ Garnet

2597

Table I. Relative density of LLZTO–xLZO (x = 0–10 wt.%) pellets sintered under different conditions

Sintering conditions	Ratio of LZO (%)					
	0	2	4	6	8	10
Relative density (%)						
1050°C × 20 h	60	65	68	64	60	61
1100°C × 10 h	77	90	89	90	85	85
1150°C × 5 h	79	90	91	91	88	87
1200°C × 2.5 h	92	92	91	92	91	91
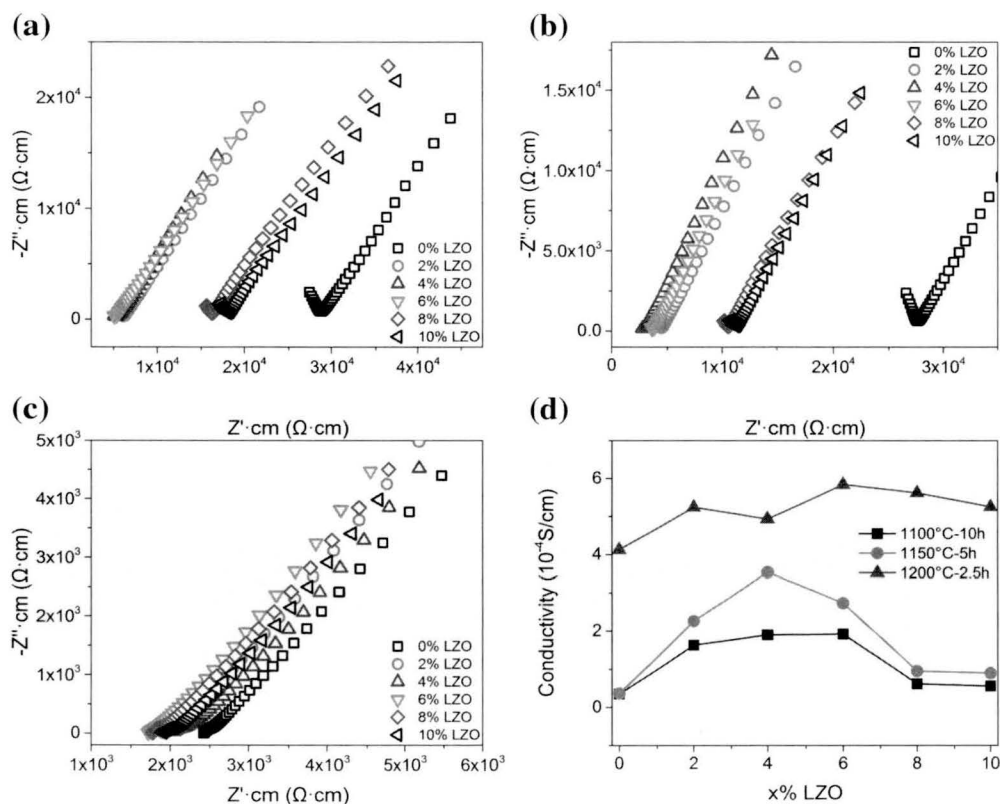
Fig. 5. AC impedance plots at 25°C of LLZTO–xLZO (x = 0–10 wt.%) pellets sintered under different conditions: (a) 1100°C × 10 h; (b) 1150°C × 5 h; (c) 1200°C × 2.5 h; (d): conductivity at 25°C versus LZO ratio.

a higher relative density than the LLZTO–0LZO samples. For pellets sintered at 1100°C, LLZTO-2, 4, 6LZO samples showed ~17% higher relative density than LLZTO–0LZO (Table I), and so did the samples sintered at 1150°C. When the temperature was elevated to 1200°C, the relative density of LLZTO–0LZO went up to 92% and fulfilled densification. The relative density of the LLZTO–2LZO pellets sintered at 1100°C and the LLZTO–6LZO pellets sintered at 1150°C was 90% and 91%, respectively, which were comparable to those of LLZTO–0LZO pellets sintered at 1200°C. These results revealed that an appropriate amount of LZO additive could effectively decrease the sintering temperature of cubic garnet LLZTO, while the high ratio of 8 wt.% or more would not be favorable.

The Nyquist plots measured at 25°C for LLZTO–xLZO (x = 0–10%) samples sintered at 1100°C × 10 h, 1150°C × 5 h and 1200°C × 2.5 h are shown in Fig. 5a, b and c, respectively. All curves showed a remarkable diffusion tail at low frequencies. The appearance of this tail in the case of Li$^+$ blocking Au electrodes demonstrates that the investigated material is intrinsically Li$^+$ conductive.[15,22] At a low sintering temperatures of 1100°C and 1150°C, the LLZTO–0LZO samples showed high resistance, and the part of semicircle which corresponds to bulk and grain boundaries can be observed in Fig. 5a and b. The resistance of the LLZTO-2, 4, 6LZO pellets sintered at 1100°C and 1150°C and of the LLZTO–xLZO (x = 0–10 wt.%) pellets sintered at 1200°C was much lower than that of the

Table II. Conductivity of LLZTO–xLZO (x = 0–10 wt.%) pellets sintered under different conditions

	Ratio of LZO (%)					
Sintering conditions	0	2	4	6	8	10
Conductivity at 25°C ($\times 10^{-4}$ S/cm)						
1100°C × 10 h	0.348	1.63	1.90	1.92	0.615	0.555
1150°C × 5 h	0.362	2.26	3.54	2.73	0.948	0.896
1200°C × 2.5 h	4.13	5.24	4.93	5.84	5.62	5.25

LLZTO–0LZO pellets sintered at 1100°C and 1150°C. No obvious response of grain and grain boundary resistance was observed in the tested frequency range within 1 MHz–10 Hz, only with an inflection point appearing before the long diffusion tail at low frequencies. The Z' value of the inflection point was determined as the total resistance of the tested samples and utilized for calculating conductivity values. As shown in Fig. 5d, the conductivity of the LLZTO–LZO pellets sintered at 1100°C and 1150°C increased as the ratio of LZO went up at first and then decreased. This result was consistent with relative density tests. As for pellets sintered at 1100°C and 1150°C, the conductivity of the LLZTO–4LZO samples was an order of magnitude higher than the pure LLZTO samples (Table II). As for pellets sintered at 1200°C, the conductivity of pellets with different ratio of LZO was at about the same level. Among them, the LLZTO–6LZO pellets showed the highest value 5.84 × 10^{-4} S/cm, which was 40% higher than that of the pure LLZTO pellets. These results clearly revealed that the LZO additive could increase the conductivity of LLZTO, indicating it as an effective sintering aid.

Microstructure and Possible Mechanism

The typical microstructure of the cross-section of the LLZO–LZO samples is shown in Fig. 6. The cross-section of the LLZTO–6LZO pellets sintered at 1150°C was much denser than the LLZTO–0LZO pellets sintered at the same temperature (Fig. 6c and d). The cross-section of the LLZTO–6LZO pellets sintered at 1150°C was as dense as the LLZTO–0LZO pellets sintered at a higher temperature of 1200°C, as shown in Fig. 6d, e, and f. These cross-section images were in agreement with relative density and conductivity results. As for pellets sintered at a low temperature, 1050°C, a lot of glass-like phases can be observed for the LLZTO–6LZO samples (Fig. 6b), while few such phases can be seen at the cross-section of the pure LLZTO samples (Fig. 6a). Grains with polyhedron surfaces were clearly observed at the cross-section of the LZO-added LLZTO samples, while round and small spheres were observed for the pure LLZTO samples. These results indicated that the LZO additive would react with some other components in the

green pellets during sintering to form low melting point glass-like phases which could play a role in the densification of LLZTO ceramics.

The components of the LLZTO–LZO green pellets were assumed to be: cubic garnet LLZTO particles with low activity, LZO, about 2 wt.% excess Li_2O, possible unreacted La_2O_3, Ta_2O_5 and ZrO_2. There was serious Li_2O loss during the sintering process,[15] meaning that the Li_2O volatilized to form a gas atmosphere. In this work, 4 wt.% excess $LiOH·H_2O$ was used to compensate the Li-loss during the high-temperature sintering process. The excessive $LiOH·H_2O$ would be dehydrated to Li_2O after 950°C × 6 h calcination process. Since the amount of LZO was based on the weight of LLZTO, the mole ratio of Li_2O to LZO in the LLZTO–4LZO green pellets would be 2 to 1. As the Li_2O in 12 g LLZNO bed powder was much more than that in the green pellets, the bed powder could provide enough volatilized Li_2O during the sintering process. Therefore, the most likely component that reacted with LZO in the green pellets should be Li_2O.

The solid-state reaction between Li_2O and LZO was conducted by sintering $LiOH·H_2O$-LZO pellets at 1150°C for 5 h with two different weight ratios of $LiOH·H_2O$ to LZO, i.e., 1:1 and 1:2. The two ratios of Li to LZO were the same as those in the LLZTO–4LZO and LLZTO–8LZO green pellets, respectively. XRD patterns for the reaction product are shown in Fig. 7. All the peaks could be ascribed to three components: cubic garnet, pyrochlore $La_2Zr_2O_7$ and Li_2ZrO_3. The intensity of the LZO varied a lot for the different ratios. Since the Li_2O was sufficient in the sample with the weight ratio of Li to LZO = 1:1, LZO could be lithiated to cubic-LLZO and Li_2ZrO_3, while Li_2O was not sufficient to lithiate LZO in the sample with the weight ratio of Li to LZO = 1:1. The proposed reaction equation is:

$$\frac{3}{2}La_2Zr_2O_7 + \frac{9}{2}Li_2O \rightarrow Li_7La_3Zr_2O_7 + Li_2ZrO_3$$
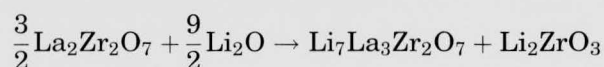
Cubic garnet $Li_7La_3Zr_2O_7$ and Li_2ZrO_3 were Li^+ conductors,[15,23] but LZO was not. Not well-lithiated LZO-based materials would be a barrier at the grain boundary for mass transport during sintering and Li^+ conducting. As a result, the relative density and conductivity for samples with a LZO ratio higher than 8 wt.% were lower than those of the LLZTO–LZO pellets with less LZO. Highly active sub-

Influence of La$_2$Zr$_2$O$_7$ Additive on Densification and Li$^+$ Conductivity for Ta-Doped Li$_7$La$_3$Zr$_2$O$_{12}$ Garnet

2599
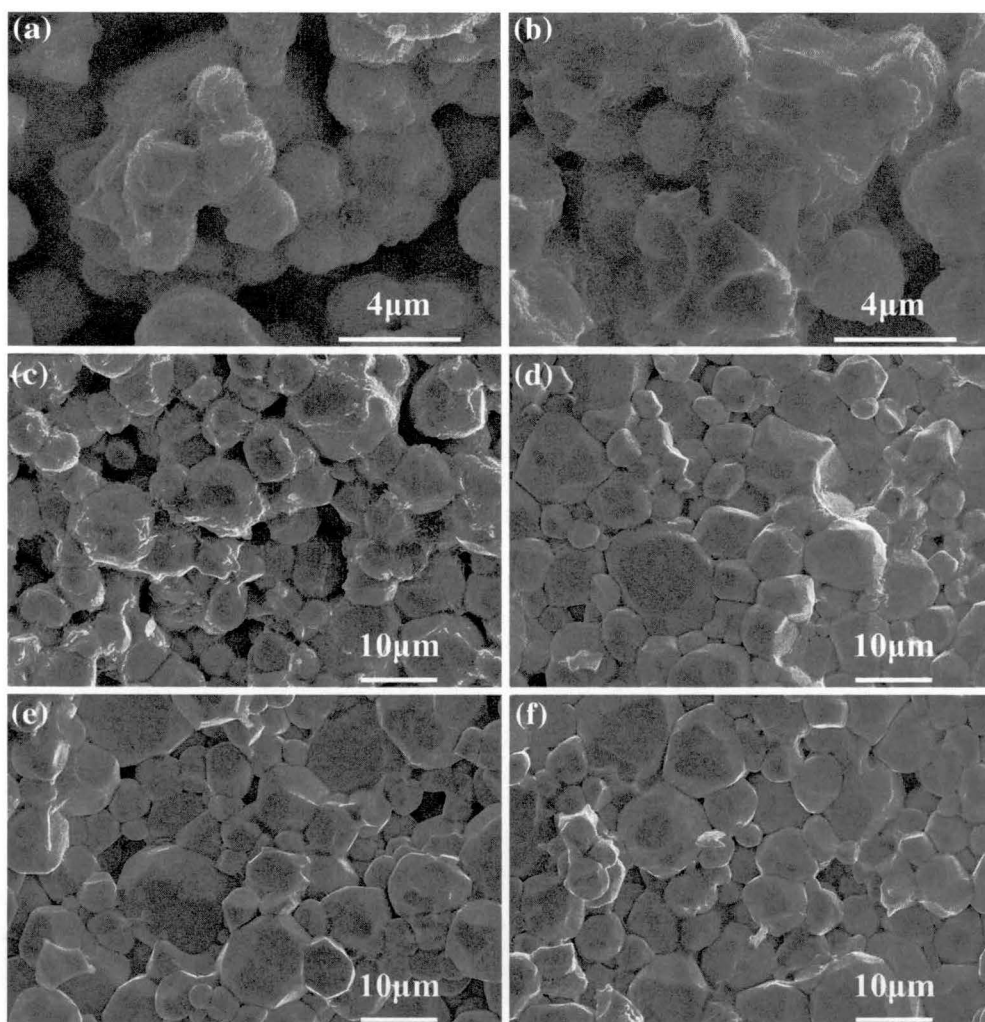
Fig. 6. (a), (c) and (e) The SEM images of LLZTO–0LZO pellets sintered at 1050°C × 20 h, 1150°C × 5 h and 1200°C × 2.5 h, respectively; (b), (d) and (f) the SEM images of LLZTO–6LZO pellets sintered at 1050°C × 20 h, 1150°C × 5 h and 1200°C × 2.5 h, respectively.
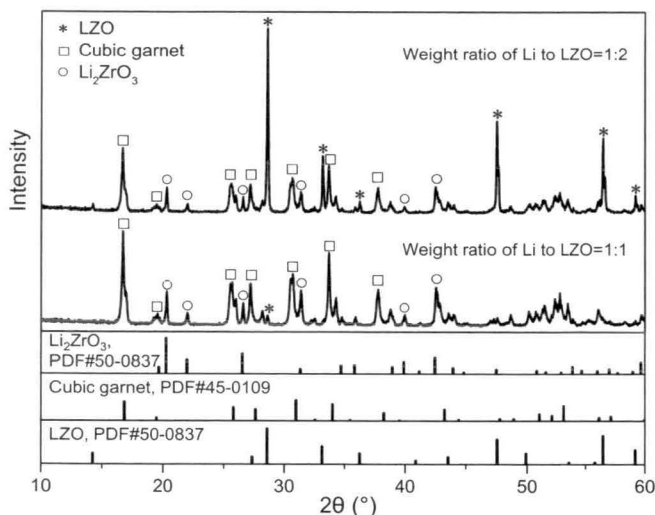
Fig. 7. XRD patterns for LiOH·H$_2$O–LZO pellets sintered at 1150°C × 5 h with different weight ratios of LiOH·H$_2$O to LZO.

micron-sized LZO would react with Li$_2$O to form glass-like phases, such as not well-crystalized LLZO and Li$_2$ZrO$_3$ or possible other low melting point materials at the grain boundaries of LLZTO acting as a sintering aid to densify the LLZTO ceramics.

CONCLUSION

Cubic garnet phase LLZTO–xLZO (x = 0–10 wt.%) samples incorporating highly active sub-micron LZO particles were successfully prepared via the conventional solid-state reaction method. The relative density of LLZTO–0LZO pellets sintered at 1100°C × 10 h and 1200°C × 2.5 h, LLZTO–6LZO pellets sintered at 1100°C × 10 h and 1150°C × 5 h was 77%, 92%, 90% and 91%, respectively, demonstrating that LLZTO could be densified at tens of degrees lower temperature with sub-micron LZO additive. The conductivity at 25°C of LLZTO–6LZO pellets sintered at 1100°C × 10 h, 1200°C × 2.5 h was 1.92×10^{-4} S/cm and 5.84×10^{-4} S/cm, which

was a magnitude and 40% higher than that of LLZTO–0LZO pellets sintered under the same conditions, respectively. Glass-like phases observed at the grain boundaries of LZO–LLZTO ceramics were supposed to be cubic $Li_7La_3Zr_2O_7$ and Li_2ZrO_3, which would help mass transport during the sintering process, leading to the enhancement of the density and conductivity of LLZTO. These results revealed that LZO is an effective sintering aid for LLZTO. Further optimization of parameters such as the granularity of the LLZTO precursor powder, the amount of LZO and the sintering process is essential to achieve denser cubic garnet LLZTO with higher conductivity for solid-state lithium batteries.

ACKNOWLEDGEMENTS

ELECTRONIC SUPPLEMENTARY MATERIAL

The online version of this article (doi:10.1007/s11837-016-2065-0) contains supplementary material, which is available to authorized users.

REFERENCES

1. J.M. Tarascon, *Philos. Trans. Ser. A Math. Phys. Eng. Sci.* 368, 3227 (2010).
2. S. Ohta, J. Seki, Y. Yagi, Y. Kihira, T. Tani, and T. Asaoka, *J. Power Sources* 265, 40 (2014).
3. Q. Wang, Z. Wen, J. Jin, J. Guo, X. Huang, J. Yang, and C. Chen, *Chem. Commun.* 52, 1637 (2016).
4. Q. Wang, J. Jin, X. Wu, G. Ma, J. Yang, and Z. Wen, *Phys. Chem. Chem. Phys.* 16, 21225 (2014).
5. Q. Wang, Z. Wen, J. Yang, J. Jin, X. Huang, W. Xiangwei, and J. Han, *J. Power Sources* 306, 347 (2016).
6. F.J. Li, H. Kitaura, and H.S. Zhou, *Energy Environ. Sci.* 6, 2302 (2013).
7. G. Adachi, N. Imanaka, and H. Aono, *Adv. Mater.* 8, 127 (1996).
8. N. Kamaya, K. Homma, Y. Yamakawa, M. Hirayama, R. Kanno, M. Yonemura, T. Kamiyama, Y. Kato, S. Hama, and K. Kawamoto, et al., *Nat. Mater.* 10, 682 (2011).
9. R. Kanno and M. Murayama, *J. Electrochem. Soc.* 148, A742 (2001).
10. C.R. Mariappan, M. Gellert, C. Yada, F. Rosciano, and B. Roling, *Electrochem. Commun.* 14, 25 (2012).
11. X. Xiaoxiong, Z. Wen, W. Xiangwei, X. Yang, and G. Zhonghua, *J. Am. Ceram. Soc.* 90, 2802 (2007).
12. X.X. Xu and Z.Y. Wen, *J. Inorg. Mater.* 20, 21 (2005).
13. S. Stramare, V. Thangadurai, and W. Weppner, *Chem. Mater.* 15, 3974 (2003).
14. V. Thangadurai, S. Narayanan, and D. Pinzaru, *Chem. Soc. Rev.* 43, 4714 (2014).
15. R. Murugan, V. Thangadurai, and W. Weppner, *Angew. Chem. Int. Ed. Engl.* 46, 7778 (2007).
16. Y.T. Li, J.T. Han, C.A. Wang, H. Xie, and J.B. Goodenough, *J. Mater. Chem.* 22, 15357 (2012).
17. I. Kokal, M. Somer, P.H.L. Notten, and H.T. Hintzen, *Solid State Ion.* 185, 42 (2011).
18. Y. Seungho, R.D. Schmidt, R. Garcia-Mendez, E. Herbert, N.J. Dudney, J.B. Wolfenstine, J. Sakamoto, and D.J. Siegel, *Chem. Mater.* 28, 197 (2016).
19. H. El Shinawi and J. Janek, *J. Power Sources* 225, 13 (2013).
20. N. Janani, C. Deviannapoorani, L. Dhivya, and R. Murugan, *RSC Adv.* 4, 51228 (2014).
21. R.P. Rao, W. Gu, N. Sharma, V.K. Peterson, M. Avdeev, and S. Adams, *Chem. Mater.* 27, 2903 (2015).
22. V. Thangadurai, R.A. Huggins, and W. Weppner, *J. Power Sources* 108, 64 (2002).
23. O.L. Andreev, M.I. Pantyukhina, B.D. Antonov, and N.N. Batalov, *Russ. J. Electrochem.* 36, 1335 (2000).